

KIC 6220497: A New Algol-type Eclipsing Binary with Multiperiodic Pulsations

Jae Woo Lee^{1,2*}, Kyeongsoo Hong¹, Seung-Lee Kim^{1,2} and Jae-Rim Koo¹

¹*Korea Astronomy and Space Science Institute, Daejeon 34113, Korea*

²*Astronomy and Space Science Major, Korea University of Science and Technology, Daejeon 34113, Korea*

Accepted 2016 ——. Received 2016 ——; in original form 2016

ABSTRACT

We present both binarity and pulsation of KIC 6220497 from the *Kepler* observations. The light curve synthesis shows that the eclipsing system is a semi-detached Algol with parameters of $q = 0.243 \pm 0.001$, $i = 77.3 \pm 0.3$ deg, and $\Delta T = 3,372 \pm 58$ K, in which the detached primary component fills its Roche lobe by $\sim 87\%$. A multiple frequency analysis of the eclipse-subtracted light residuals reveals 33 frequencies in the range of $0.75\text{--}20.22$ d^{−1} with amplitudes between 0.27 and 4.56 mmag. Among these, four are pulsation frequencies in fundamental (f_1, f_5) and p (f_2, f_7) modes, and six are orbital frequency (f_8, f_{31}) and its harmonics ($f_6, f_{11}, f_{20}, f_{24}$), which can be attributed to tidally excited modes. For the pulsation frequencies, the pulsation constants of $0.16\text{--}0.33$ d and the period ratios of $P_{\text{pul}}/P_{\text{orb}} = 0.042\text{--}0.089$ indicate that the primary component is a δ Sct pulsating star and, thus, KIC 6220497 is an oscillating eclipsing Algol (oEA) star. The dominant pulsation period of 0.1174051 ± 0.0000004 d is significantly longer than that expected from empirical relations that link the pulsation period with the orbital period. The surface gravity of $\log g_1 = 3.78 \pm 0.03$ is clearly smaller than those of the other oEA stars with similar orbital periods. The pulsation period and the surface gravity of the pulsating primary demonstrate that KIC 6220497 would be the more evolved EB, compared with normal oEA stars.

Key words: binaries: eclipsing - stars: fundamental parameters - stars: individual (KIC 6220497) - stars: oscillations (including pulsations).

1 INTRODUCTION

δ Sct stars are main sequence and subgiant stars with spectral types from about A2 to F2 (Rodríguez & Breger 2001). They pulsate in low-order radial/non-radial pressure (p) modes with short periods of $0.02\text{--}0.2$ d (Breger 2000). The pulsations are driven by the κ mechanism acting in the He II partial ionization region. Recently, Balona (2014) showed that nearly all δ Sct stars pulsate in the frequency range of $0\text{--}5$ d^{−1} characteristic of γ Dor stars and suggested that the low frequencies are directly associated with the presence of δ Sct pulsations. The δ Sct and γ Dor variables share a similar parameter space in the Hertzsprung-Russell (HR) diagram which is partly overlapped, but the latter stars pulsate in high-order non-radial gravity (g) modes driven by a mechanism known as convective blocking (Guzik et al. 2000) with relatively longer periods of $0.4\text{--}3$ d (Handler & Shobbrook 2002; Henry, Fekel & Henry 2005). The hybrid stars that contain the p and g modes simultaneously are of particular interest, since they probe both the envelope and the deep interior near the core region of the pulsators (Kurtz et al. 2015).

Over 90 pulsating stars have been known as the δ Sct, γ Dor, and hybrid stars in eclipsing binaries (EBs). Approximately 73 of them are the so-called oEA (oscillating eclipsing Algol) stars; the mass-accreting components of classical semi-detached Algols that lie inside the instability strip and show δ Sct-like oscillations (Mkrtichian et al. 2004). The δ Sct stars in EBs exhibit almost the same pulsating characteristics as single δ Sct pulsators, but their evolutionary processes are entirely different from each other by tidal interaction and mass transfer between components. For the pulsating EBs, a possible relation between the binary orbital periods (P_{orb}) and the dominant pulsation periods (P_{pul}) was firstly given by Soyduğan et al. (2006) and updated by Liakos et al. (2012): $P_{\text{pul}} = 0.020P_{\text{orb}} - 0.005$ for 20 EBs and $\log P_{\text{pul}} = 0.58P_{\text{orb}} - 1.53$ for 70 EBs in the same order. Later, the $P_{\text{pul}} - P_{\text{orb}}$ relation was theoretically established by Zhang, Luo & Fu (2013), in which the pulsation period

* E-mail: jwlee@kasi.re.kr

could be described as a function of the orbital period, the pulsation constant, the mass ratio, and the filling factor. According to those studies, the eclipsing δ Sct stars pulsate with shorter pulsational periods than single δ Sct pulsators. The pulsational period seems to depend on the gravitational force exerted by a companion onto the pulsating star. This indicates that the companion star may influence the pulsation frequencies and modes of the pulsating component. The pulsating stars in EBs offer a unique opportunity to study the effects of tidal forces and companions on the pulsations (Hambleton et al. 2013), as well as to measure directly the masses and radii of the pulsators from binary modelling.

The EBs with pulsating stars are the Rosetta stone for the study of stellar structure and evolution through asteroseismology and binary properties. Such examples are KIC 10661783 (Southworth et al. 2011; Lehmann et al. 2013), KIC 4544587 (Hambleton et al. 2013), and KIC 3858884 (Maceroni et al. 2014). Because space missions such as *Kepler* and *CoRoT* provide ultra-precise photometric data, they allow the detection of many pulsation frequencies with amplitudes down to the micro-magnitude level. In order to look for pulsating components in EBs and to understand their physical properties, we choose the *Kepler* target KIC 6220497 (R.A.₂₀₀₀ = 19^h44^m39^s.547; decl.₂₀₀₀ = +41°33′21″17; K_p = +14.749; g = +14.935; $g - r$ = +0.247), which was announced to be probably a pulsating EB with an orbital period of 1.323 d by Gaulme & Guzik (2014). This paper is the third contribution in a series assessing the detections and properties of pulsating stars in the *Kepler* EBs (Lee et al. 2014, 2016). Here, we present the binary system as an oEA star showing multiperiodic δ Sct pulsations, based on light-curve synthesis and frequency analysis for the light residuals from the binary model.

2 KEPLER PHOTOMETRY AND LIGHT-CURVE SYNTHESIS

KIC 6220497 was observed during Quarters 14 and 15 in the long cadence mode, which has a sampling time of 29.4 min. We used the data in the *Kepler* EB catalogue¹ detrended and normalised from the raw SAP (Simple Aperture Photometry) time series (Prša et al. 2011; Slawson et al. 2011). The contamination level of the measurements is estimated to be 0.046. This value suggests that the *Kepler* target suffers minimally from third light, if any. Figure 1 depicts the *Kepler* light curve for KIC 6220497, where there are no significant trends in the eclipse depths and the light maxima (Max I and Max II) present equal light levels. As shown in the phase-folded light curve, the binary star displays a considerable variation outside eclipses due to tidal distortions. The depth difference between the primary and secondary eclipses indicates a large temperature difference between the component stars.

For the light-curve synthesis of KIC 6220497, we used the 2007 version of the Wilson-Devinney synthesis code (Wilson & Devinney 1971, van Hamme & Wilson 2007; hereafter W-D). The *Kepler* data of this system were analysed in a manner almost identical to that for the pulsating EBs V404 Lyr (KIC 3228863; Lee et al. 2014) and KIC 4739791 (Lee et al. 2016). The effective temperature (T_1) of the brighter, and presumably more massive, star was initialised to be 7,254 K from the *Kepler* Input Catalogue (KIC; Kepler Mission Team 2009). The logarithmic bolometric ($X_{1,2}$) and monochromatic ($x_{1,2}$) limb-darkening coefficients were interpolated from the values of van Hamme (1993). The gravity-darkening exponents were fixed at standard values of $g_1=1.0$ and $g_2=0.32$, while the bolometric albedos at $A_1=1.0$ and $A_2=0.5$, as surmised from the components' temperatures. Adjustable parameters were the orbital ephemeris (T_0 and P), the mass ratio (q), the orbital inclination (i), the effective temperatures ($T_{1,2}$) and the dimensionless surface potentials ($\Omega_{1,2}$) of the components, and the monochromatic luminosity (L_1). This synthesis was repeated until the correction of each adjustable parameter became smaller than its standard deviation using the differential correction (DC) programme of the W-D code. In this paper, the subscripts 1 and 2 refer to the primary and secondary components being eclipsed at Min I and Min II, respectively.

The mass ratio ($q = M_2/M_1$) is a very important parameter in the light-curve synthesis. However, there exist neither photometric solutions nor spectroscopic orbits for KIC 6220497. Because the binary star is a faint object with a short orbital period, 8–10 m class telescopes are needed to measure its radial velocities. However, it is very difficult to obtain such observation times. Thus, we conducted an extensive q -search procedure, meaning that we calculated a series of models with the mass ratios in step of 0.01 between 0.1 and 1.0. For each assumed mass ratio, the DC programme was applied for various modes but showed acceptable photometric solutions only for semi-detached mode 5 in which the secondary component fills its inner Roche lobe. As displayed in Figure 2, the q searches indicate that the minimum value of the weighted sum of the squared residuals ($\sum W(O - C)^2$; hereafter \sum) is around $q = 0.24$. In the subsequent calculations, this q value was treated as an adjustable parameter. The result is listed in the second and third columns of Table 1 and appears as a solid curve in the right panel of Figure 1. The light residuals from Model 1 are plotted as the grey circles in the lower panel of Figure 3, wherein it can be seen that the model light curves describe the *Kepler* data satisfactorily.

The photometric solutions for Model 1 could be affected by the multiperiodic pulsations of the primary component, which will be discussed in the following section. We removed the pulsation signatures from the original *Kepler* data, leaving behind the light variations due to binarity effects. Then, the new light curve was solved by using Model 1 as initial values. The final result is illustrated in Figure 3, and is given as Model 2 in the fourth and fifth columns of Table 1. As listed in the table, the binary parameters for Model 2 are in good agreement with those for Model 1. We can see that the photometric solutions of KIC 6220497 are immune from the light variation due to the pulsations. Our light-curve synthesis represents KIC 6220497 as a semi-detached eclipsing system in which the primary component fills its limiting lobe by $\Omega_1/\Omega_{in} = 87\%$, where Ω_{in} is the potential for the inner critical surface. The Roche-geometry configuration of the system permits some mass transfer from

¹ <http://keplerebs.villanova.edu/>

the lobe-filling secondary to the detached primary component. In all the procedures that have been described, we included the orbital eccentricity (e) as a free parameter but found that the parameter remained indistinguishable from zero within its error. This indicates that KIC 6220497 is in a circular orbit, as expected for semi-detached classical Algols.

It is known that the standard errors of the adjustable parameters taken from the W-D code are unrealistically small because of the strong correlations between relatively many parameters and partly the non-normal distribution of measurement errors (Maceroni & Rucinski 1997). In order to obtain more reliable errors for the Model 1 and Model 2 parameters, we followed the procedure described by Koo et al. (2014). First of all, we divided the observed (or prewhitened) *Kepler* data of KIC 6220497 into 138 segments at the interval of an orbital period and separately analysed them with the W-D code. Then, we computed the standard deviations of each parameter from the 138 different values. The parameter errors presented in Table 1 are the 1σ -values adopted from this procedure.

The temperatures of the primary component in Table 1 correspond to a normal main-sequence star with a spectral type of A9. Because the temperature errors are certainly underestimated, it was assumed that the temperature of each component had an error of 200 K. Using the correlations between spectral type and stellar mass (Harmanec 1988), we estimated the primary's mass to be $M_1 = 1.60 \pm 0.08 M_\odot$. The absolute dimensions for KIC 6220497 can be computed from our photometric solutions and M_1 . These are given in the bottom of Table 1, where the radii are the mean volume radii calculated from the tables of Mochnacki (1984). The luminosities and the bolometric magnitudes were computed by adopting $T_{\text{eff}\odot} = 5780$ K and $M_{\text{bol}\odot} = +4.73$ for solar values.

3 LIGHT RESIDUALS AND PULSATONAL CHARACTERISTICS

In order to obtain more reliable frequencies, the observed *Kepler* data were split into 138 subsets as before and modeled individually with the W-D code through adjusting only the ephemeris epoch (T_0) in the Model 1 of Table 1. The light residuals from the analyses are displayed in Figure 4 as magnitudes versus BJDs, wherein the lower panel presents a short section of the residuals. Light variations with a total peak-to-peak amplitude of ~ 10 mmag are clearly seen in the residuals. In order to examine the oscillating features, we applied a multiple frequency analysis to the whole data sets at once. The PERIOD04 programme by Lenz & Breger (2005) was performed on the frequency range from 0 to the Nyquist limit of 24.47 d^{-1} . Because the primary component lies within the δ Sct instability strip of the HR diagram, it would be a candidate for such pulsations. During primary eclipses, the secondary component partially blocks the lights of the pulsating primary star, which can have an effect on the observed frequencies and amplitudes. In contrast, the light contribution from the secondary is only 2.2 % to the total luminosity of the binary system, so the pulsations are almost unaffected during the secondary eclipses. Thus, we made use of only the light residuals having orbital phases between 0.12 and 0.88 after eliminating the data of the primary eclipses.

The amplitude spectra for KIC 6220497 are shown in the top panel of Figure 5. After the successive prewhitening of each frequency peak, we detected 33 frequencies with the signal to noise amplitude (S/N) ratios larger than 4.0 (Breger et al. 1993). At each step of this procedure, a multiperiodic least-squares fit to the light residuals was carried out using the fitting formula of $Z = Z_0 + \sum_i A_i \sin(2\pi f_i t + \phi_i)$. Here, Z and Z_0 denote the calculated magnitude and zero point, respectively, A_i and ϕ_i are the amplitude and phase of the i th frequency, respectively, and t is the time of each measurement. The amplitude spectra after prewhitening the first seven frequencies and then all 33 frequencies are presented in the middle and bottom panels of Figure 5, respectively. The results are presented in Table 2, where the uncertainties were calculated according to Kallinger, Reegen & Weiss (2008). The synthetic curve obtained from the 33-frequency fit is displayed in the lower panel of Figure 4. Some additional peaks still exist in the bottom panel of Figure 5, but their S/N ratios are smaller than the empirical threshold of 4.0.

As in the case of KIC 4739791 (Lee et al. 2016), to see if the main frequencies detected in this paper are real and stable during the observing run of ~ 200 d, we re-analysed the light residuals at intervals of about 50 d and examined the frequency variations with time. The four subsets resulted in slight differences from each other and approximate 20 frequencies were detected at each subset with the same criterion of $S/N > 4.0$. Figure 6 showed the stability of the 14 frequencies. Among these, the four frequencies ($f_9, f_{10}, f_{14}, f_{21}$) varied significantly and the three frequencies decreased (f_3, f_{16}) or increased (f_{17}) monotonically. Within the frequency resolution of 0.008 d^{-1} (Loumos & Deeming 1978), we checked the frequencies for possible harmonic and combination terms. The result is listed in the last column of Table 2, where the six ($f_6, f_8, f_{11}, f_{20}, f_{24}, f_{31}$) frequencies are the orbital frequency ($f_{\text{orb}} = 0.75576 \text{ d}^{-1}$) and its harmonics.

4 DISCUSSION AND CONCLUSIONS

In this paper, we studied the physical properties of KIC 6220497 from detailed analyses of the *Kepler* time-series data obtained during Quarters 14 and 15. The *Kepler* light curve was satisfactorily modelled for two cases: including and removing pulsations. The binary parameters between them are consistent with each other, which indicates that the photometric analysis of KIC 6220497 is almost unaffected by pulsations. The light-curve synthesis presented in this paper demonstrates that the system is a semi-detached EB with parameters of $q = 0.243 \pm 0.001$, $i = 77.3 \pm 0.3$ deg, and $\Delta T = 3,372 \pm 58$ K. The detached primary component is about 1.6 times larger than the lobe-filling secondary and fills its inner critical lobe by about 87%, which is one of the largest filling factors for pulsating EBs. In Figure 7, a comparison of the KIC 6220497 parameters with the mass-radius,

mass-luminosity, and HR diagrams shows that the primary star lies in the main-sequence band, while the secondary is highly evolved and its radius and luminosity are more than four times oversized and about 26 times overluminous, respectively, compared with dwarf stars of the same mass. In these diagrams, the locations of both components conform to the general pattern of semi-detached Algols (İbanoğlu et al. 2006).

For the detection of the pulsation frequencies in KIC 6220497, we removed the binarity effects from the observed *Kepler* data and performed a frequency analysis in the entire light residuals, excluding the data around the primary minima. As a consequence, we detected the 33 frequencies including a dominant oscillation found at $f_1 = 8.51752 \pm 0.00003 \text{ d}^{-1}$, corresponding to $0.1174051 \pm 0.0000004 \text{ d}$. Among these, the four (f_1, f_2, f_5, f_7) frequencies in the p -mode region were highly stable during the observing runs of about 200 d. On the contrary, the other frequencies varied with time and/or may be orbital harmonics and combination terms. The frequency ratio of f_1 and f_5 is 0.984, very close to 1.0, and these frequencies could not be interpreted by two radial modes of δ Sct stars (Breger 1979). We checked the ratios of the other frequencies and found one candidate to be identified as radial modes, i.e. the ratio of 0.848 between f_2 and f_7 is nearly the same with the period ratio of 0.845 for the second (2H) and third (3H) overtone radial modes of the δ Sct stars. It means that the longer period f_7 could be classified as the second overtone radial mode and the shorter period f_2 as the third overtone radial mode. Applying the physical parameters of the primary component in Table 1 to the equation of $\log Q_i = -\log f_i + 0.5 \log g + 0.1 M_{\text{bol}} + \log T_{\text{eff}} - 6.456$ (Breger 2000), we obtained the pulsation constants for the four frequencies ($f_{1,2,5,7}$) to be $Q_1 = 0.033 \text{ d}$, $Q_2 = 0.016 \text{ d}$, $Q_5 = 0.033 \text{ d}$, and $Q_7 = 0.019 \text{ d}$. We compared these Q values with the theoretical models with $1.5 M_{\odot}$ given by Fitch (1981). The f_1 and f_5 frequencies could be identified as fundamental ($n = 0$) modes and the f_2 and f_7 as the third ($n = 3$) and second ($n = 2$) overtone p -modes, respectively. The ratios, $P_{\text{pul}}/P_{\text{orb}} = 0.042 \sim 0.089$, of the pulsational to orbital periods are within the upper limit of $P_{\text{pul}}/P_{\text{orb}} = 0.09 \pm 0.02$ for δ Sct stars in EBs that could be used to distinguish approximately whether a binary component pulsates in the p -mode (Zhang, Luo & Fu 2013). These results indicate that the primary star with a spectral type of A9V can be classified as a δ Sct variable. Because the system is in a semi-detached configuration, these results imply that KIC 6220497 would be an oEA star and a mass transfer from the evolved lobe-filling secondary to the detached primary component could be responsible for the δ Sct-type pulsations detected in this paper.

The oEA stars have pulsation features similar to classical δ Sct stars. However, their pulsations may be influenced by the tidal interaction and mass transfer between the components, as well as gravitational force from companions. Some pulsations in KIC 6220497 can be excited by the tidal forces of the secondary companion. Tidally excited modes occur when the orbital frequency is close to a stellar eigenfrequency in a binary star with an eccentric orbit. The signature of the pulsation modes is the frequencies at integer multiples of the orbital frequency (Welsh et al. 2011; Thompson et al. 2012; Hambleton et al. 2013). We detected four ($f_6, f_{11}, f_{20}, f_{24}$) frequencies that are the harmonics of the orbital frequency, which could be partly affected by imperfect removal of the eclipses from the light curve. Although the orbit of the binary system is circular, these frequencies could result from tidally induced pulsations (Reyniers & Smeyers 2003a,b; Southworth et al. 2011). In the upper panel of Figure 8, we plot the dominant pulsation period versus the orbital period for 74 oEA stars, including KIC 6220497. The data are taken from the compilations of Zhang, Luo & Fu (2013; 67 oEA stars) and from more recent literature (Yang, Wei & Li 2014 for FR Ori; Zhang et al. 2014 for OO Dra; Zhang, Luo & Wang 2015 for EW Boo; Zhang et al. 2015 for V392 Ori; Lee et al. 2016 for KIC 4739791; Soyduğan et al. 2016 for XZ Aql). In the panel, we can see that the pulsation period of KIC 6220497 deviated from the general trend of the oEA stars and also the empirical relation between P_{pul} and P_{orb} of Zhang, Luo & Fu (2013). The pulsation periods in EBs increase with decreasing gravitational pull exerted by the secondary companion to the pulsating primary component (Soyduğan et al. 2006). For KIC 6220497, the gravitational pull applied to per gram of the matter on the surface of the pulsating component by the lobe-filling secondary was calculated to be $\log F = 2.90$ in cgs units, which is about 3.4 times smaller than the value of 9.89 (again, in cgs units) taken from the relation of $\log P_{\text{pul}} = -0.61 \log F + 5.1$ calibrated by Soyduğan et al. (2006). However, as shown in the lower panels of Figure 8 from 34 oEA stars currently known, the gravitational force $\log F$ for KIC 6220497 matches well with those for the other oEA stars with similar orbital periods, while the surface gravity $\log g_1 = 3.78$ for the primary component is clearly smaller. The period-gravity relation is similar to that for radially pulsating stars suggested by Fernie (1995); as the surface gravity decreases, its pulsation period increases. Further, it is known that the more evolved the star, the slower the pulsations (cf. Liakos et al. 2012). The pulsation period and the surface gravity of KIC 6220497 indicate that the system might be a more evolved EB than the other oEA stars. We think that the pulsation periods strongly depend on the surface gravities of the pulsating components and the evolutionary status of the binary stars.

When the double-lined radial velocities and the multiband light curves are made (e.g., Hong et al. 2015, Koo et al. 2016), they will help to understand the absolute parameters, identification of pulsation modes, and evolutionary status of KIC 6220497 better than now. These offer us important information for asteroseismology and the study of stellar interior and evolution.

ACKNOWLEDGMENTS

We appreciate the careful reading and valuable comments of the anonymous referee. This paper includes data collected by the *Kepler* mission. *Kepler* was selected as the 10th mission of the Discovery Program. Funding for the *Kepler* mission is provided by the NASA Science Mission directorate. We have used the Simbad database maintained at CDS, Strasbourg, France. This work was supported by the KASI (Korea Astronomy and Space Science Institute) grant 2016-1-832-01.

REFERENCES

- Balona L. A., 2014, MNRAS, 437, 1476
- Breger M., 1979, PASP, 91, 5
- Breger M., 2000, in ASP Conf. Ser. 210, Delta Scuti and Related Stars, ed. M. Breger and M. Montgomery (San Francisco: ASP), 3
- Breger M., Stich J., Garrido R. et al., 1993, A&A, 271, 482
- Fernie J. D., 1995, AJ, 110, 2361
- Fitch W. S., 1981, ApJ, 249, 218
- Gaulme P., Guzik J. A., 2014, in Proc. IAU Symp. 301, Precision Asteroseismology, ed. J. A. Guzik, W. Chaplin, G. Handler, & A. Pigulski (Cambridge: Cambridge Univ. Press), 413
- Guzik J. A., Kaye A. B., Bradley P. A., Cox A. N., Neuforge C., 2000, ApJ, 542, L57
- Handler G., Shobbrook R. R., 2002, MNRAS, 333, 251
- Hambleton K. M., Kurtz D. W., Prša A. et al., 2013, MNRAS, 434, 925
- Harmanec P., 1988, Bull. Astron. Inst. Czechoslovakia, 39, 329
- Henry G. W., Fekel F. C., Henry S. M., 2005, AJ, 129, 2815
- Hong K., Lee J. W., Kim S.-L. et al., 2015, AJ, 150, 131
- İbanoğlu C., Soyduğan F., Soyduğan E., Dervişoğlu A., 2006, MNRAS, 373, 435
- Kallinger T., Reegen P., Weiss W. W., 2008, A&A, 481, 571
- Kepler Mission Team 2009, VizieR Online Data Catalog, 5133, 0
- Kurtz D. W., Hambleton K. M., Shibahashi H., Murphy S. J., Prša A., 2015, MNRAS, 446, 1223
- Koo J.-R., Lee J. W., Lee B.-C. et al., 2014, AJ, 147, 104
- Koo J.-R., Lee J. W., Hong K. et al., 2016, AJ, 151, 77
- Lee J. W., Kim S.-L., Hong K., Lee C.-U., Koo J.-R., 2014, AJ, 148, 37
- Lee J. W., Kim S.-L., Hong K., Koo J.-R., Lee C.-U., Youn J.-H., 2016, AJ, 151, 25
- Lehmann H., Southworth J., Tkachenko A., Pavlovski K., 2013, A&A, 557, 79
- Lenz P., Breger M., 2005, Comm. Asteroseismology, 146, 53
- Liakos A., Niarchos P., Soyduğan E., Zasche P., 2012, MNRAS, 422, 1250
- Loumos G. L., Deeming T. J., 1978, Ap&SS, 56, 285
- Maceroni C., Lehmann H., da Silva R. et al., 2014, A&A, 563, 59
- Maceroni C., Rucinski S. M., 1997, PASP, 109, 782
- Mkrtichian D. E., Kusakin A. V., Rodríguez E. et al., 2004, A&A, 419, 1015
- Mochmacki S. W., 1984, ApJS, 55, 551
- Prša A., Batalha N., Slawson R. W. et al., 2011, AJ, 141, 83
- Reyniers K., Smeyers P., 2003a, A&A, 404, 1051
- Reyniers K., Smeyers P., 2003b, A&A, 409, 677
- Rodríguez E., Breger M., 2001, A&A, 366, 178
- Slawson R. W., Prša A., Welsh W. F. et al., 2011, AJ, 142, 160
- Southworth J., Zima W., Aerts C. et al., 2011, MNRAS, 414, 2413
- Soyduğan E., İbanoğlu C., Soyduğan F., Akan M. C., Demircan O., 2006, MNRAS, 366, 1298
- Soyduğan E., Soyduğan F., Aliçavuş F., Erdem A., 2016, New Astron., 46, 40
- Thompson S. E., Everett M., Mullally F. et al., 2012, ApJ, 753, 86
- Tout C. A., Pols O. R., Eggleton P. P., Han Z., 1996, MNRAS, 281, 257
- Van Hamme W., 1993, AJ, 106, 209
- Van Hamme W., Wilson R. E., 2007, ApJ, 661, 1129
- Welsh W. F., Orosz J. A., Aerts C. et al., 2011, ApJS, 197, 4
- Wilson R. E., Devinney E. J., 1971, ApJ, 166, 605
- Yang Y.-G., Wei J.-Y., Li H.-L. 2014, AJ, 147, 35
- Zhang X. B., Deng L. C., Tian J. F. et al., 2014, AJ, 148, 106
- Zhang X. B., Luo C. Q., Fu J. N., 2013, ApJ, 777, 77
- Zhang X. B., Luo Y. P., Wang K., 2015, AJ, 149, 96
- Zhang X. B., Luo Y. P., Wang K., Luo, C. Q. 2015, AJ, 150, 37

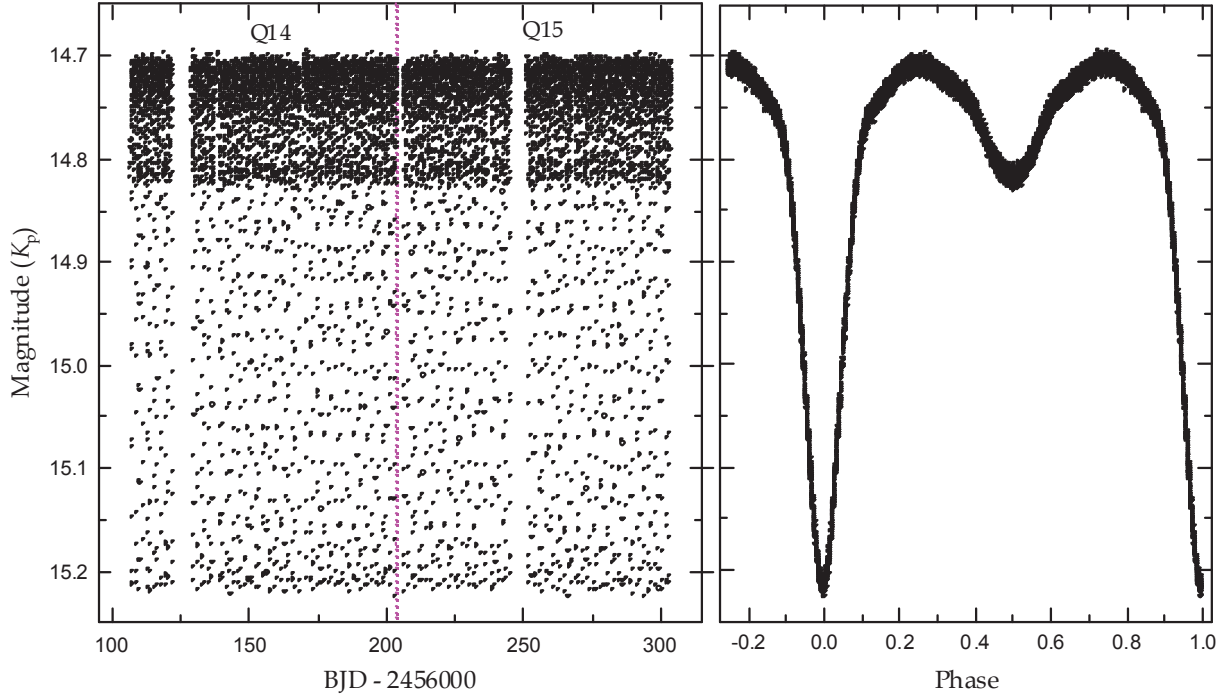


Figure 1. Observed *Kepler* light curve of KIC 6220479 distributed in BJD (left panel) and orbital phase (right panel). In the left panel, the vertical dashed line represents the ending time of Quarter 14.

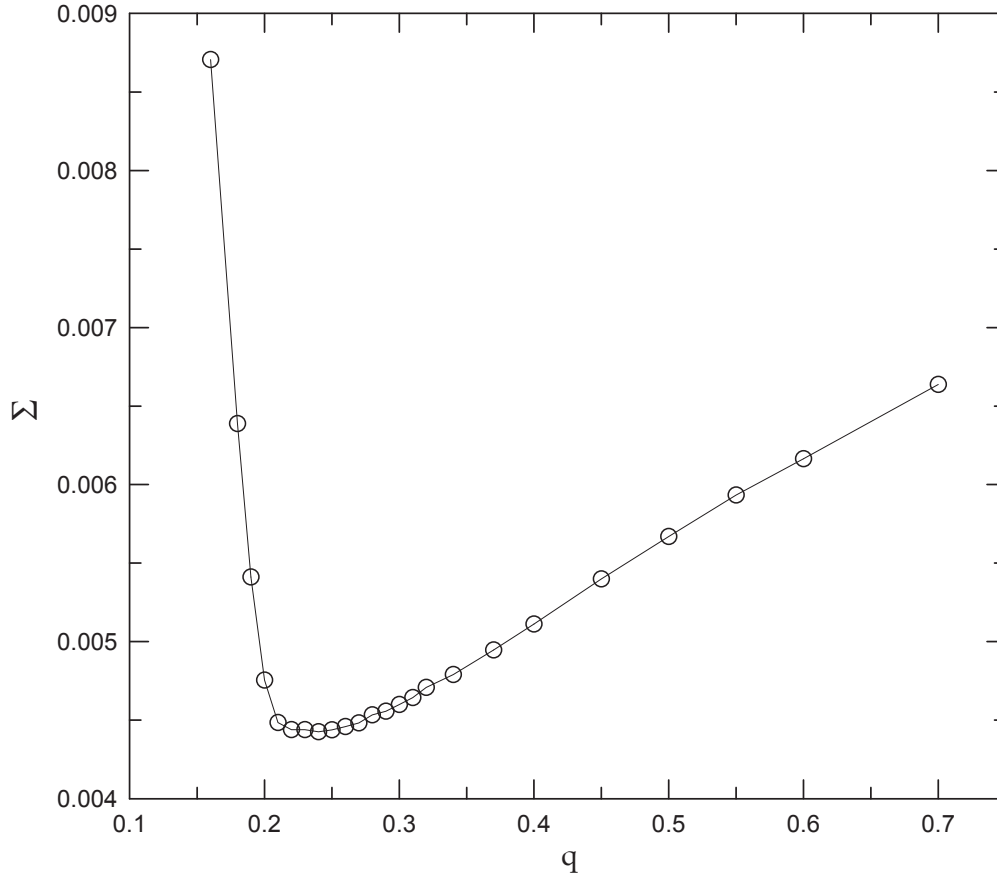


Figure 2. Behaviour of \sum (the sum of the residuals squared) of KIC 6220497 as a function of mass ratio q , showing a minimum value at $q=0.24$. The circles represent the q -search results for each assumed mass ratio.

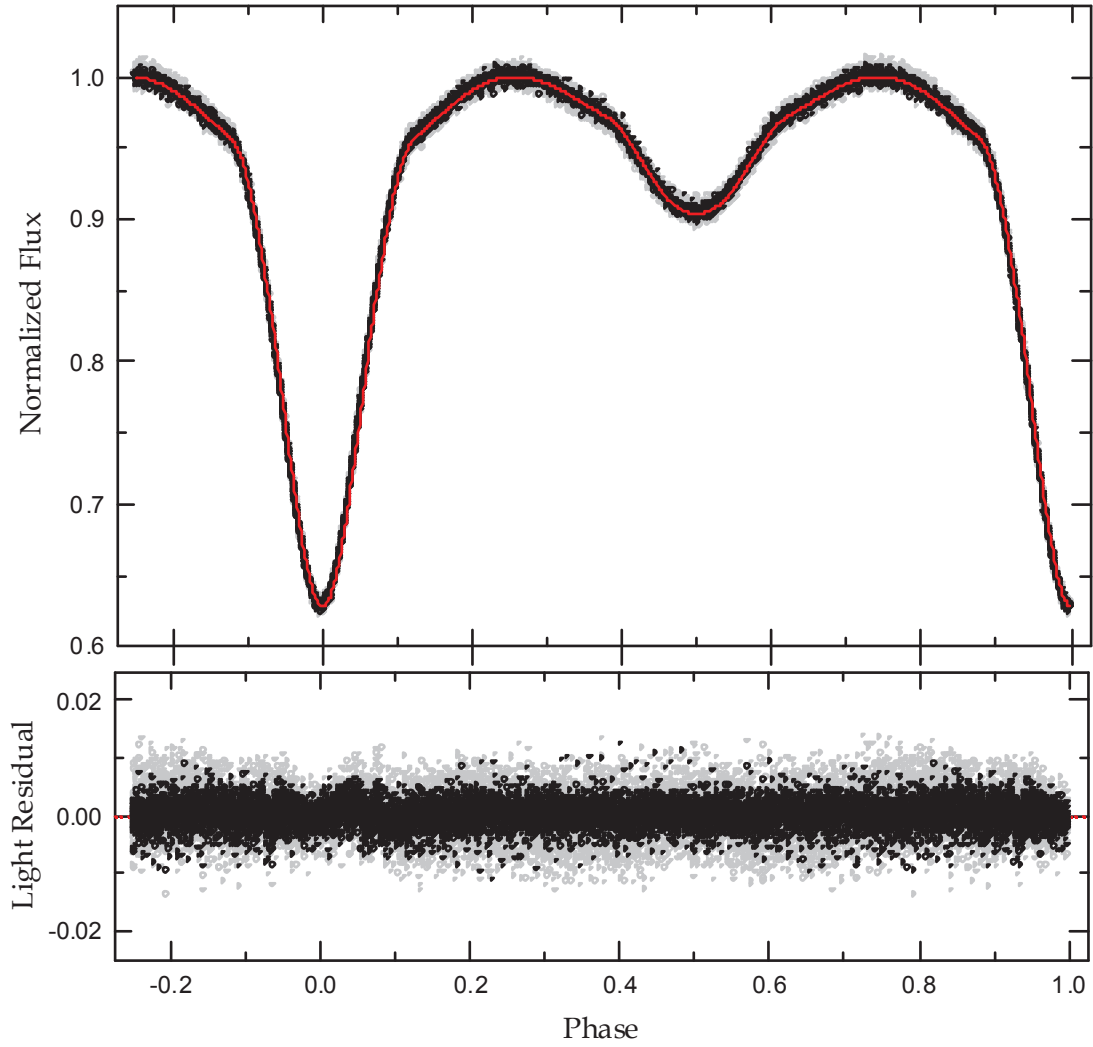


Figure 3. Binary light curve (black circle) after subtracting the pulsation signatures from the observed *Kepler* data (grey circle). In the upper panel, the blue dashed and red solid curves are computed with the Model 1 and Model 2 parameters of Table 1, respectively. Because the two models are in substantial agreement with each other, the fitted Model 1 cannot be seen individually. The lower panel represents the light residuals from both datasets: observed and prewhitened light curves.

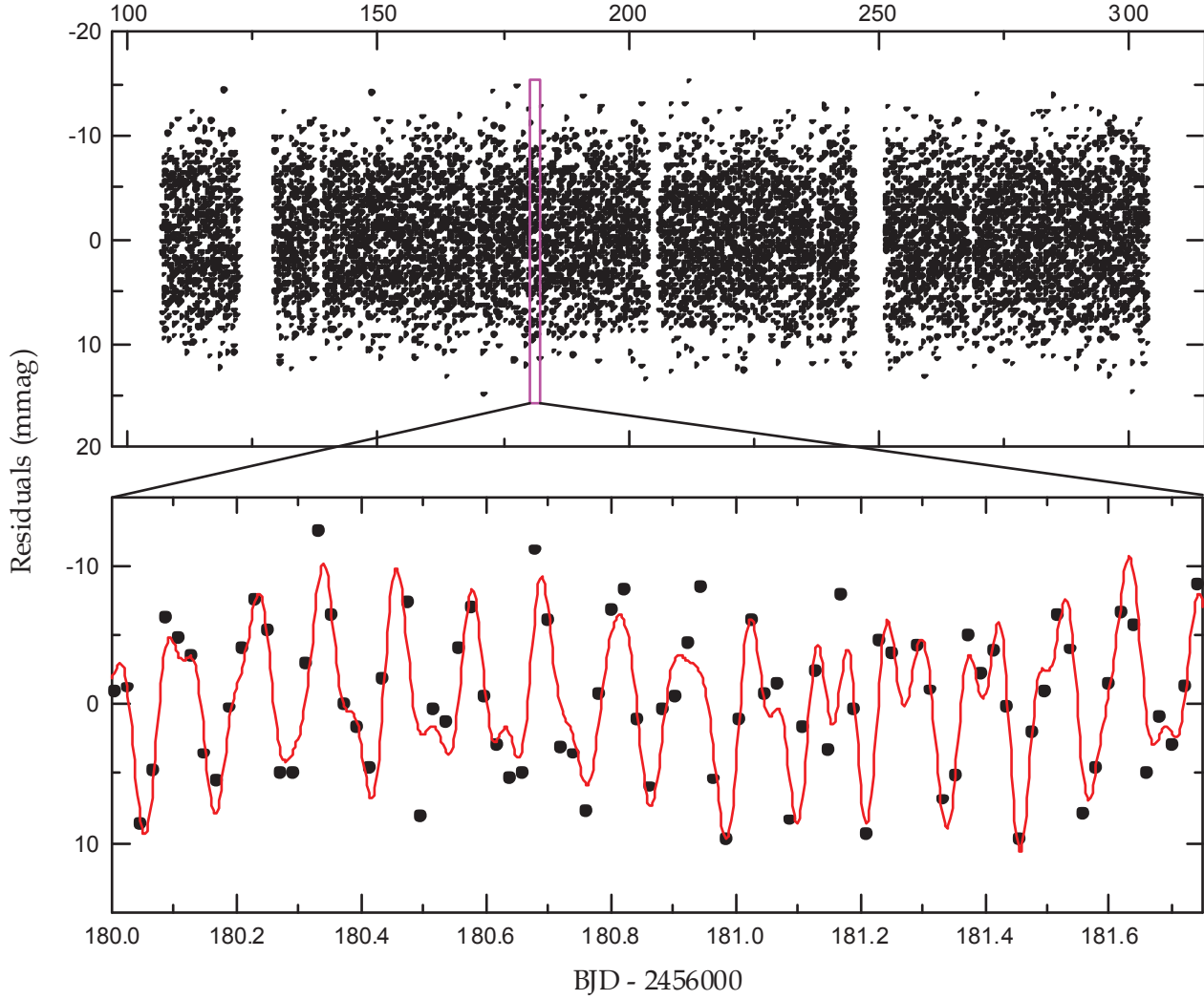


Figure 4. Light residuals after subtracting the binarity effects from each of the 138 light curves in the original *Kepler* data. The lower panel presents a short section of the residuals marked using the inset box of the upper panel. The synthetic curve was computed from the 33-frequency fit to the data between orbital phases 0.12 and 0.88.

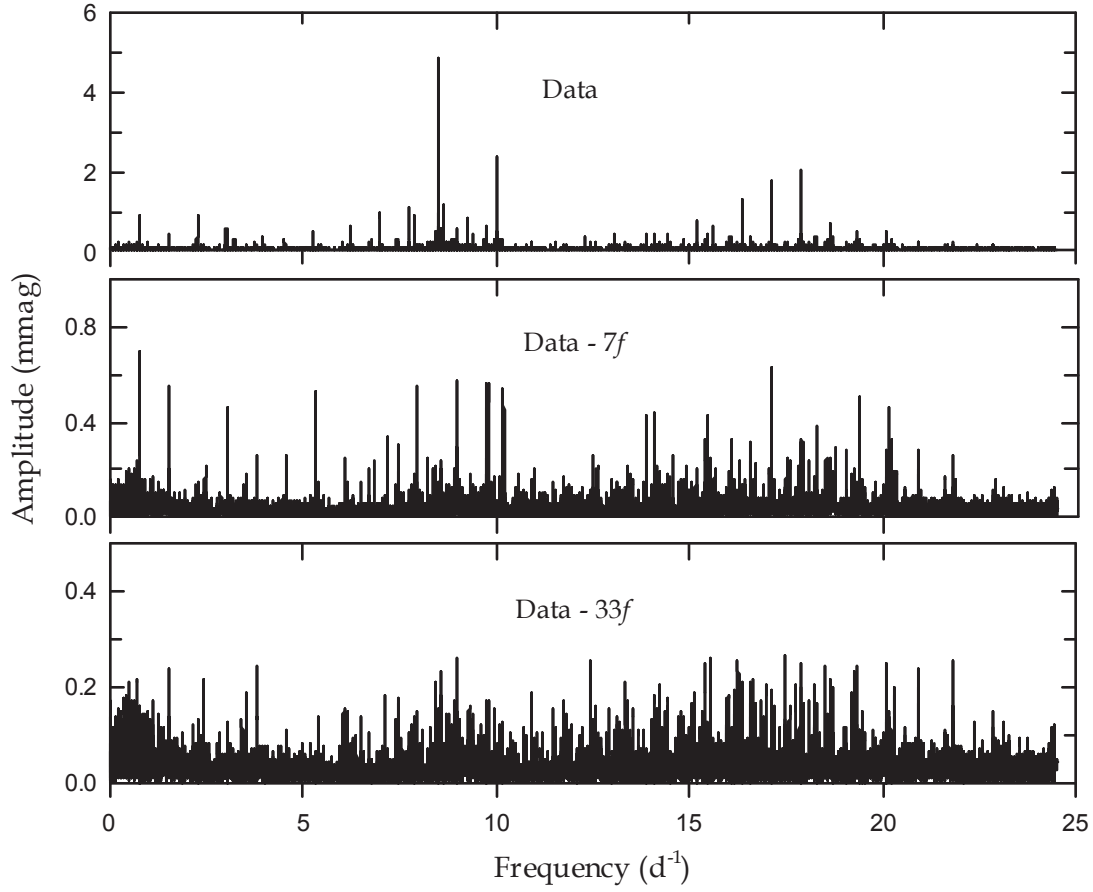


Figure 5. Amplitude spectra before (top panel) and after prewhitening the first 7 frequencies (middle panel) and all 33 frequencies (bottom panel) from the PERIOD04 programme. The frequency analysis was applied to the entire *Kepler* data except for the times of the primary eclipses.

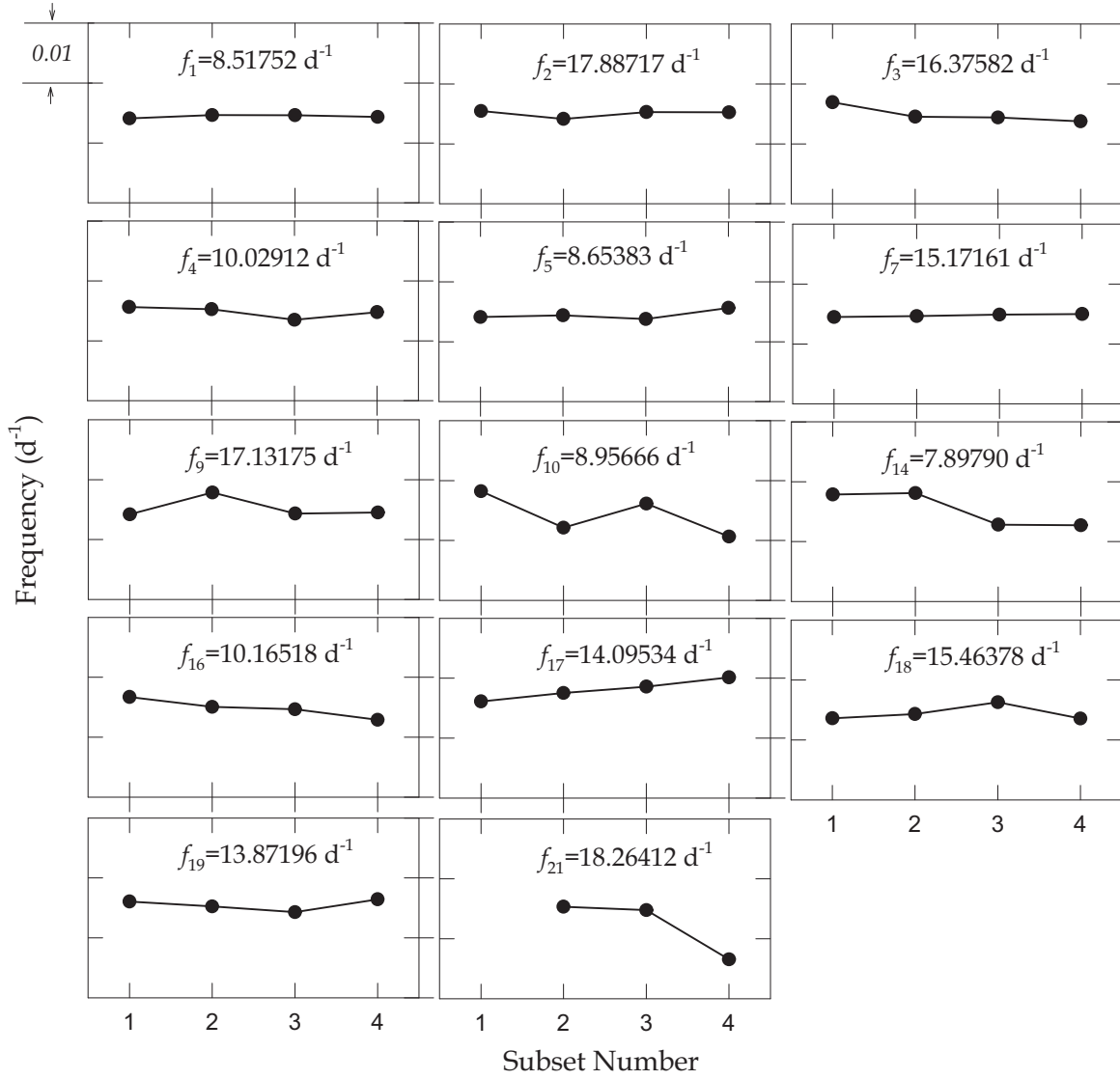


Figure 6. Variability of the main frequencies detected in the four subsets at intervals of approximately 50 d. In all panels, the y-axes are scaled to 0.03 d^{-1} , and the tick intervals are 0.01 d^{-1} .

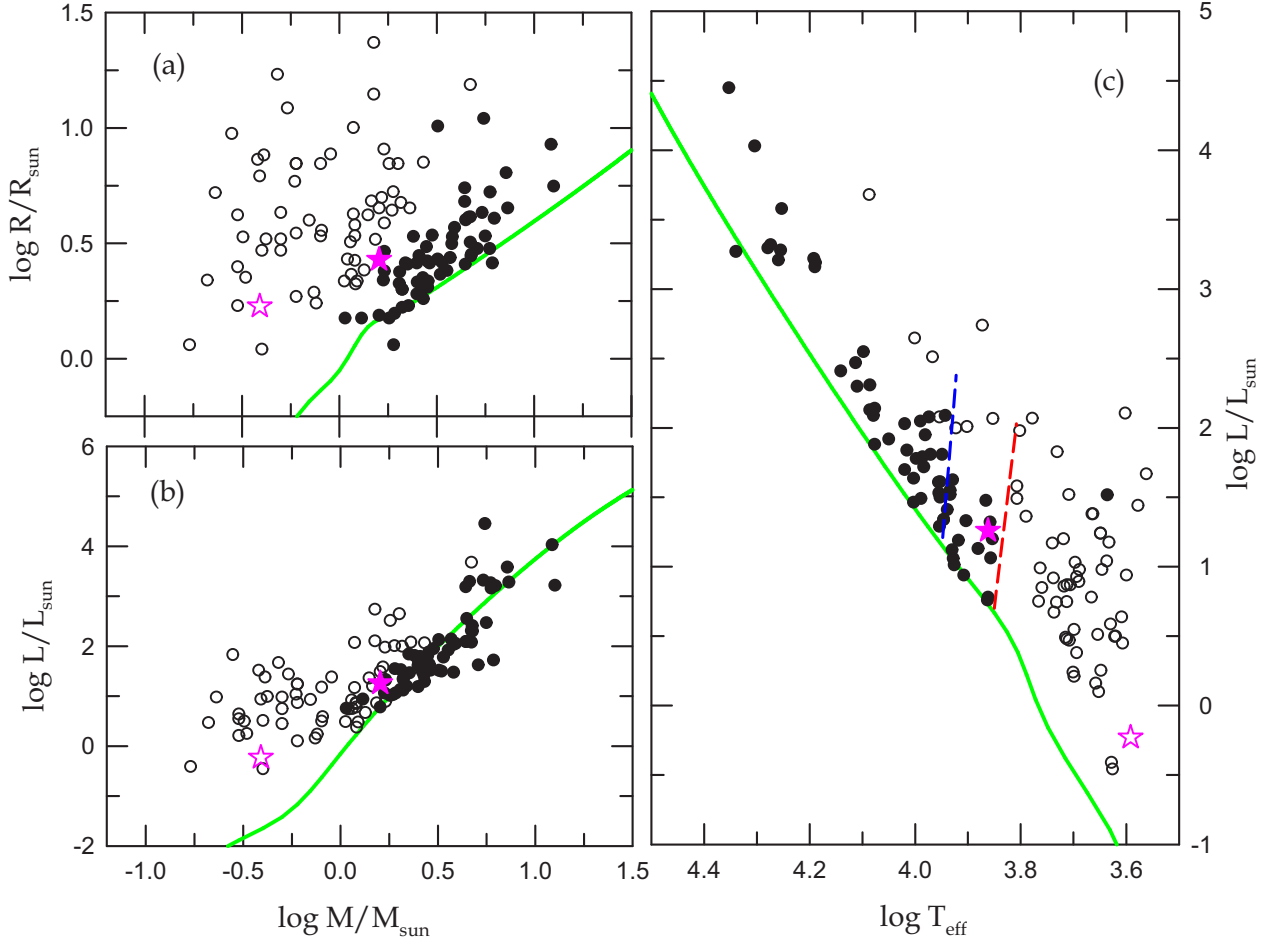


Figure 7. Plots of (a) mass-radius, (b) mass-luminosity, and (c) HR diagrams for semi-detached Algols (İbanoğlu et al. 2006). The filled and open circles represent the primary and secondary components, respectively. The filled and open star symbols denote the locations of the primary and secondary components of KIC 6220497, respectively, and the solid lines represent the ZAMS stars calculated as having a solar metallicity of $Z=0.02$ found in Tout et al. (1996). In panel (c), the dashed blue and red lines represent the theoretical edges of the δ Sct instability strip, and the pulsating primary star of KIC 6220497 resides within the region.

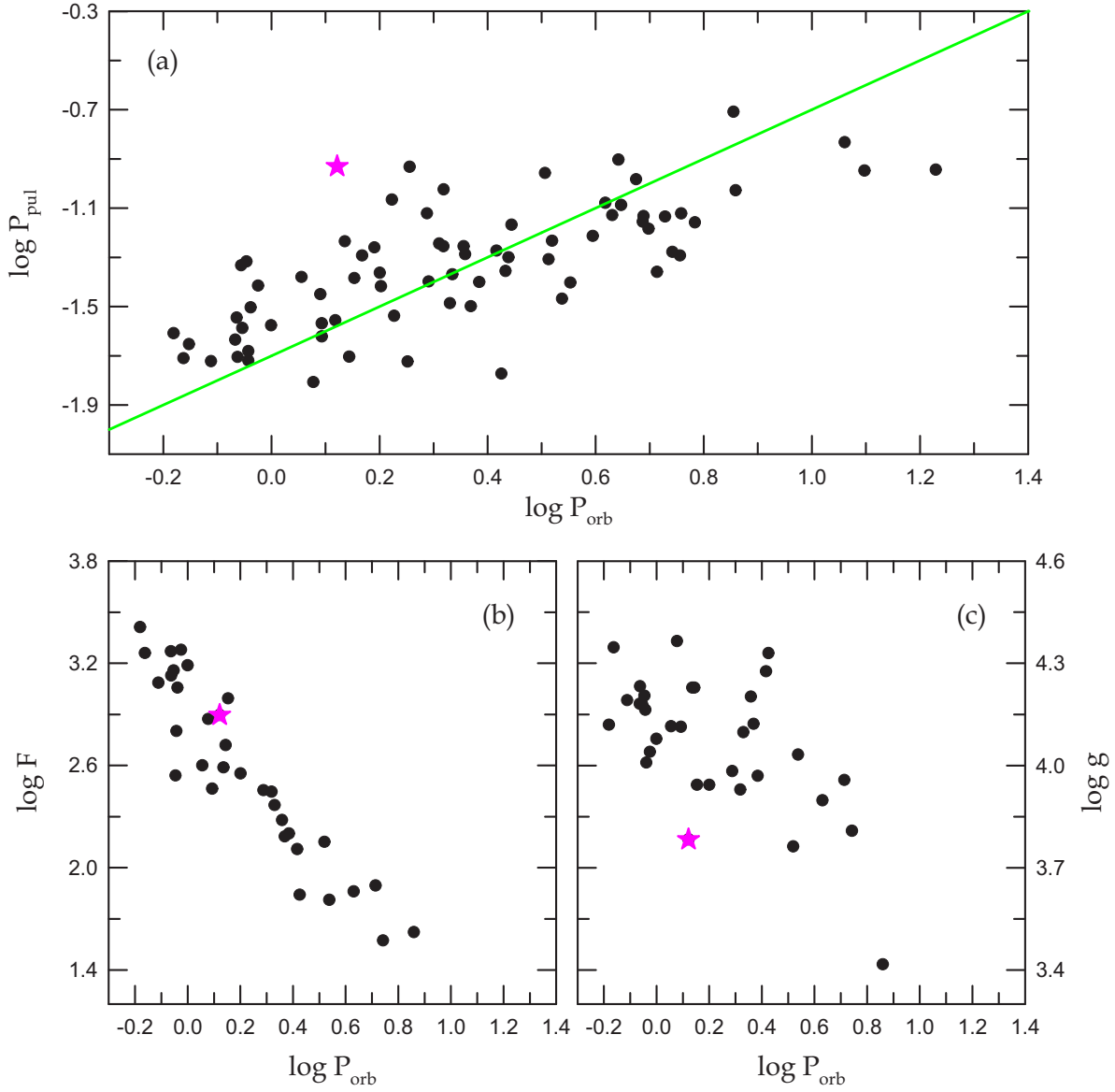


Figure 8. Plots of (a) pulsation periods $\log P_{\text{pul}}$, (b) the gravitational forces $\log F$, and (c) surface gravities $\log g$ against the orbital periods P_{orb} for oEA stars. The star symbols denote the parameters of KIC 6220497, and the solid line in the upper panel represents the relation of $\log P_{\text{pul}} = \log P_{\text{orb}} - 1.70$ given by Zhang, Luo & Fu (2003). See text for details.

Table 1. Binary Parameters of KIC 6220497.

Parameter	Model 1 ^a		Model 2 ^b	
	Primary	Secondary	Primary	Secondary
T_0 (BJD)	2,456,204.39612(5)		2,456,204.39619(2)	
P (day)	1.323167(1)		1.3231670(6)	
q	0.242(3)		0.243(1)	
i (deg)	77.3(1.6)		77.3(3)	
T (K)	7,263(64)	3,911(20)	7,279(54)	3,907(22)
Ω	2.688(13)	2.335	2.689(7)	2.336
A	1.0	0.5	1.0	0.5
g	1.0	0.32	1.0	0.32
X, Y	0.640, 0.259	0.621, 0.150	0.640, 0.259	0.621, 0.150
x, y	0.598, 0.260	0.751, 0.026	0.598, 0.258	0.750, 0.026
$L/(L_1+L_2)$	0.978(2)	0.022	0.978(2)	0.022
r (pole)	0.4060(15)	0.2460(9)	0.4058(11)	0.2462(6)
r (point)	0.4479(28)	0.3590(12)	0.4477(18)	0.3593(8)
r (side)	0.4251(18)	0.2560(9)	0.4249(14)	0.2562(6)
r (back)	0.4356(22)	0.2885(9)	0.4355(15)	0.2888(6)
r (volume) ^c	0.4224(18)	0.2644(9)	0.4223(13)	0.2646(6)
$\sum W(O - C)^2$	0.0044		0.0023	
Absolute parameters:				
M (M_\odot)	1.60(8)	0.39(2)	1.60(8)	0.39(2)
R (R_\odot)	2.69(6)	1.68(4)	2.69(6)	1.69(4)
$\log g$ (cgs)	3.78(3)	3.57(3)	3.78(3)	3.57(3)
L (L_\odot)	18(2)	0.6(1)	18(2)	0.6(1)
M_{bol} (mag)	1.6(1)	5.3(2)	1.6(1)	5.3(2)

^a Result from the observed *Kepler* light curve.^b Result from the prewhitened light curve removing the pulsations.^c Mean volume radius.This paper has been typeset from a \LaTeX file prepared by the author.

Table 2. Multiple Frequency Analysis of KIC 6220497^a.

	Frequency (day ⁻¹)	Amplitude (mmag)	Phase (rad)	S/N ^b	Remark
f_1	8.51752±0.00003	4.56±0.15	6.24±0.10	52.39	
f_2	17.88717±0.00006	2.19±0.13	0.77±0.18	28.07	
f_3	16.37582±0.00009	1.56±0.13	4.78±0.25	20.25	$f_2 - 2f_{\text{orb}}$
f_4	10.02912±0.00010	1.41±0.14	2.51±0.30	16.79	$f_1 + 2f_{\text{orb}}$
f_5	8.65383±0.00014	1.11±0.15	2.04±0.39	12.75	
f_6	2.26728±0.00015	0.62±0.09	5.71±0.43	11.59	$3f_{\text{orb}}$
f_7	15.17161±0.00014	0.81±0.11	5.44±0.41	12.16	
f_8	0.75567±0.00014	0.78±0.11	3.52±0.40	12.60	f_{orb}
f_9	17.13175±0.00017	0.81±0.13	2.53±0.48	10.34	$f_2 - f_{\text{orb}}$
f_{10}	8.95666±0.00025	0.60±0.15	4.52±0.72	6.96	
f_{11}	5.29073±0.00014	0.58±0.08	1.02±0.40	12.67	$7f_{\text{orb}}$
f_{12}	9.73721±0.00026	0.56±0.14	0.40±0.75	6.68	$3f_{10} - f_2 + f_{\text{orb}}$
f_{13}	9.75701±0.00026	0.56±0.14	2.62±0.75	6.65	$3f_1 - 2f_5 + 2f_{\text{orb}}$
f_{14}	7.89790±0.00029	0.52±0.15	3.94±0.83	6.05	$f_5 - f_{\text{orb}}$
f_{15}	19.35892±0.00030	0.40±0.12	1.45±0.87	5.77	
f_{16}	10.16518±0.00030	0.49±0.14	4.76±0.86	5.80	$f_5 + 2f_{\text{orb}}$
f_{17}	14.09534±0.00023	0.44±0.10	1.38±0.67	7.43	
f_{18}	15.46378±0.00029	0.44±0.13	3.94±0.83	6.04	
f_{19}	13.87196±0.00023	0.42±0.09	3.35±0.66	7.57	
f_{20}	3.02371±0.00019	0.44±0.09	3.39±0.56	8.94	$4f_{\text{orb}}$
f_{21}	18.26412±0.00033	0.40±0.13	3.16±0.95	5.28	$7f_{10} - 2f_2 - f_5$
f_{22}	16.05471±0.00040	0.32±0.13	0.39±1.17	4.28	
f_{23}	17.88336±0.00037	0.37±0.13	3.48±1.06	4.73	
f_{24}	6.80183±0.00037	0.35±0.13	6.22±1.06	4.73	$9f_{\text{orb}}$
f_{25}	20.11434±0.00032	0.34±0.11	5.61±0.92	5.48	
f_{26}	7.43718±0.00042	0.32±0.13	1.67±1.23	4.09	$f_{10} - 2f_{\text{orb}}$
f_{27}	16.57356±0.00042	0.32±0.13	5.63±1.23	4.09	
f_{28}	18.73168±0.00042	0.30±0.13	6.26±1.23	4.09	$2f_2 - 2f_1$
f_{29}	19.03705±0.00040	0.30±0.12	2.67±1.16	4.32	
f_{30}	20.21511±0.00035	0.30±0.10	5.89±1.02	4.93	
f_{31}	0.75212±0.00036	0.30±0.11	0.67±1.04	4.80	f_{orb}
f_{32}	20.06306±0.00039	0.27±0.11	6.26±1.13	4.43	$2f_1 + 4f_{\text{orb}}$
f_{33}	14.52484±0.00039	0.27±0.10	4.58±1.13	4.42	$f_2 - f_5 + 7f_{\text{orb}}$

^a Frequencies are listed in order of detection.^b The noise was calculated in a range of 5 d⁻¹ around each frequency.